Achievable high Voc of carbon based all-inorganic CsPbIBr2 perovskite solar cells through interface engineering

Journal Name

ARTICLE

Achievable high V_{oc} of carbon based all-inorganic $CsPbIBr_2$ perovskite solar cells through interface engineering

Zhanglin Guo, Siowhwa Teo, Zhenhua Xu, Chu Zhang, Yusuke Kamata, Shuzi Hayase, Tingli Ma*

Received 00th January 20xx,
Accepted 00th January 20xx

DOI: 10.1039/x0xx00000x

www.rsc.org/

In this work, a simple interface engineering process for SnO_2 electron selective layer (ESL) surface passivation employing $SnCl_2$ solution is introduced, where it has successfully reduced the energy loss for high open-circuit voltage (V_{oc}) output and consequently improved the performance of the all-inorganic $CsPbIBr_2$ perovskite solar cells (PSCs). It was found that the surface passivation can effectively suppress the recombination process at the interface between the perovskite and the SnO_2 due to higher recombination resistance. The shorter PL decay time is dedicated to the more excellent electron extraction from the perovskite film. After optimizing the surface passivation, the power conversion efficiency (PCE) was enhanced from 4.73% to 7.00% and a high V_{oc} of 1.31 V was achieved, which is one of the highest V_{oc} reported for the inorganic Cs-based PSCs. More importantly, the passivated SnO_2 based device retains 95.5% of its initial performance at 90 °C in the air without encapsulation. This work provides a simple and efficient interface engineering method to improve the V_{oc} and efficiency of all-inorganic PSCs.

Introduction

Organic-inorganic hybrid perovskite solar cells (PSCs) have been attracting tremendous attention in the past several years, leading to an achievable high power conversion efficiency (PCE) of 23.3%.[1, 2] The perovskite light absorber, in most highly efficiency PSCs, is composed of the organic cations (e.g., methylammonium (MA) and formamidinium (FA)) hybridizing with the lead halide frameworks, which promises perfect band gap and strong light absorption ability.[3-5] However, the thermal stability of these hybrid PSCs is an important issue to be addressed owing to the irreversible decomposition of the perovskite phase to lead iodide and organic molecules when exposure to heat stress at low temperature (80 °C).[6] Mixing the inorganic Caesium (Cs) with the MA and FA can improve the composition and structural tolerability to higher temperature (100 °C).[7] While the fundamental solution for the thermal endurance is to entirely replace the organic cations with a Cs cation. Thus the inorganic PSCs with the formula of $CsPbX_3$ (X=I, Br) are attracting great attention due to their outstanding thermal stability (stable over 400 °C) and high-speed progression in their performance.[8-11]

Among the family of $CsPbX_3$, the $CsPbBr_3$ is the most stable one, but its large band gap (2.30 eV) leads to poor light absorbing ability.[12] The narrowest band gap $CsPbI_3$ possesses good light absorbing property but easily transforms to non-photoactive orthorhombic phase (yellow phase) at room temperature in air.[10, 13, 14] Therefore, for balancing the band gap and the phase stability of $CsPbX_3$ perovskite materials, mixing I and Br is one of the best choices.[11] For example, $CsPbIBr_2$ is a good light absorber with a proper band gap of 2.0 eV and better phase stability at room temperature. However, the performance of the $CsPbIBr_2$ based PSCs is still low. One crucial factor is the open-circuit voltage (V_{oc}) owing to large energy losses (E_{loss}), which is defined as the energy loss between the bandgap of the perovskite materials and the device V_{oc} ($E_{loss}= E_g-eV_{oc}$).[8] For example, Yabing Qi et al. fabricated the all-inorganic $CsPbIBr_2$ based PSCs with carbon electrode and the V_{oc} is only 0.96 V (PCE=6.14%) with the E_{loss} of larger than 1.0 eV, which is much larger than that of the organic-inorganic PSCs (less than 0.5 eV).[15] Zhong Jin and co-workers also fabricated a similar device structure with the V_{oc} of 1.08 V.[16] Higher V_{oc} for $CsPbIBr_2$ based device of 1.227 V was achieved by Yibing Cheng et al., in which they utilized Spiro-OMeTAD hole transporting materials (HTM) and Au electrode, and achieved a PCE of 8.02%.[17] Thus the E_{loss} must be reduced in order to further improve the performance of the inorganic PSCs. It has been proven that non-radiative recombination at the interface between the perovskite film and the electron selective layer (ESL) or HTM, is one of the major factors that induce E_{loss} of the device.[8] For instance, Qifan Xue et al. constructed SnO_2/ZnO bilayered ESL for $CsPbI_2Br$, which has successfully suppressed interfacial trap-assisted recombination and contributed to a high V_{oc} of 1.23 V and PCE of 14.6%.[8] Alex K.-Y. Jen and co-workers modified the SnO_2 film by C60 and the resultant V_{oc} and PCE of $CsPbIBr_2$ are 1.18 V and 7.34%, respectively.[18] Therefore, interface engineering is a very promising method to reduce the E_{loss}, and to increase V_{oc} for further enhancement of all-inorganic PSCs's performances.

Here we propose a simple interface engineering process for SnO_2 ESL surface passivation employing $SnCl_2$ solution. It shows that surface passivation leads to faster carrier transformation through the interface and larger charge recombination resistance for the $CsPbIBr_2$ PSCs. By employing the passivated SnO_2 ESL, a high V_{oc} of

Graduate School of Life Science and Systems Engineering, Kyushu Institute of Technology, Kitakyushu, Fukuoka 808-0196, Japan

*(*Corresponding author: tinglima@life.kyutech.ac.jp)*

† Footnotes relating to the title and/or authors should appear here.
Electronic Supplementary Information (ESI) available: [details of any supplementary information available should be included here]. See DOI: 10.1039/x0xx00000x

1.31 V was recorded for the $CsPbIBr_2$ PSCs using the carbon as the counter electrode. The PCE was enhanced from 4.73 to 7.00 % after the passivation process. Our results indicate that surface passivation is a very promising method to reduce the E_{loss} for the all-inorganic PSCs.

Results and discussion

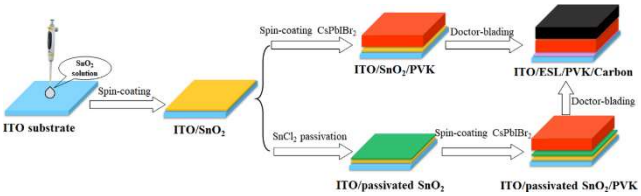

Fig. 1 Fabrication process of all-inorganic PSCs with bare or passivated SnO_2 ESL.

Fig. 1 shows the fabrication process of the all-inorganic PSCs where the bare and passivated SnO_2 were used as the ESL (The details are depicted in Experiment Section in supplementary information). Firstly, we spin-coated the SnO_2 colloid (tin (IV) oxide) solution to form the SnO_2 film. The ultra-thin passivation SnO_2 layer was prepared by spin-coating 0.1 M $SnCl_2$ precursor on the prepared SnO_2 at 6000 rpm followed by an annealing process at 180 ^oC for 1 h. Fig. 2 shows the field emission scanning electron microscope (SEM) images and the atomic force microscope (AFM) images of the SnO_2 film before and after passivation. From Fig. 2a and c, we can confirm that the introduction of ultra-thin passivation SnO_2 layer induces a significant difference in the film morphology. Several prominent holes are observed from the SnO_2 film (red-circled), implying an imperfect coverage property, which will lead to severe recombination during the charge extraction from the perovskite film. While, with an ultra-thin passivation SnO_2 layer, the holes are filled; this forms a hole-free ESL. We also compared them by AFM images as shown in Fig. 2b and d. The SnO_2 film becomes much smoother after passivated by $SnCl_2$. Specifically, the root-square-roughness (Rq) is dramatically decreased from 7.05 nm to 4.21 nm, which implies the effect of passivation. The effect of passivated or non-passivated is also presented in Fig. S1, as observed through their transmittance properties. Comparing with the bare SnO_2 film, the films passivated by $SnCl_2$ with different concentrations display higher transmittance properties in the visible light region. This phenomenon is attributed to the formation of the smoother surface, which leads to lower reflectivity and thus higher transmittance.[19] The SnO_2 film passivated with 0.15 M $SnCl_2$ has the highest transmittance because of its smoother surface and lower Rq of 2.99 nm (Fig. S2). The smoother surface is resulted from the passivation effect rather than annealing at higher temperature of 180 ^oC, as shown in Fig. S3.

In order to investigate the effect of SnO_2 film passivation on the performance of the devices, we fabricated an inorganic $CsPbIBr_2$ perovskite film on bare and passivated SnO_2 film, respectively. The fabrication process is shown in Fig. 1 and what should be noted is that the inorganic $CsPbIBr_2$ film was annealed at a relatively low temperature of 160 ^oC, rather than the widely used temperature of around 300 ^oC in previous publications.

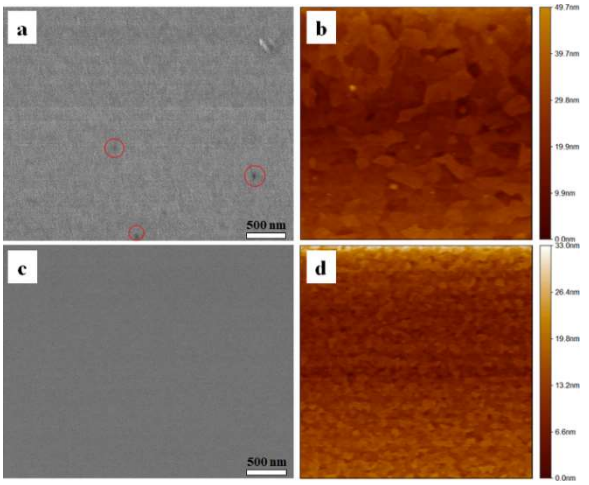

Fig. 2 Top-view SEM images of (a) bare and (c) passivated SnO_2 films; AFM images of the (b) bare and (d) passivated SnO_2 films.

Fig. S4 shows the X-ray diffraction (XRD) patterns of the $CsPbIBr_2$ films on different ESLs and the insets illustrate the photographs of the prepared $CsPbIBr_2$ film. From the XRD patterns, we found that both the films show similar strong peaks at 14.7^o, 20.9^o, 29.9^o, corresponding to (100), (110), and (200) crystal planes of the $CsPbIBr_2$ cubic perovskite structure, respectively.[20-22] Moreover, as shown in Fig. S5, both the $CsPbIBr_2$ films display similar surface morphologies, but the film on passivated SnO_2 seems a little denser with higher coverage owing to the smoother surface of ESL, which is a beneficial criterion to form a high-quality perovskite layer.[23] The effects of SnO_2 passivation on the cell performance are further investigated by fabricating PSCs with the architecture of ITO/ESL/$CsPbIBr_2$/Carbon, as depicted in Fig. 1, in which the ESL is bare SnO_2 or passivated SnO_2 film.

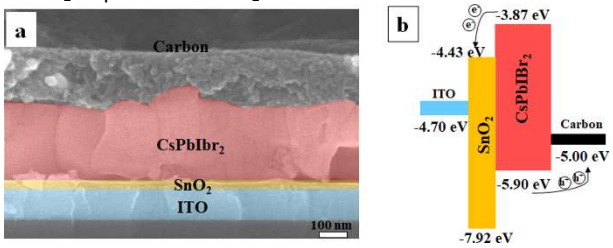

Fig. 3 (a) Cross-section SEM image and (b) energy diagram of the components of the all-inorganic $CsPbIBr_2$ PSCs.

Fig. 3a shows the cross-section SEM image with passivated SnO_2 ESL and the thickness of the perovskite layer is about 260 nm, which is similar to those of previous reports.[15, 16, 18] Therefore, we confirm that through the processes depicted in Fig. 1, the above architecture was successfully fabricated. Moreover, the band alignment diagram of the components (Fig. 3b), determined from Fig. S6, illustrates that the light-generated electrons and holes can be effectively transferred from the perovskite absorber to the ESL and the HTM, respectively, implying perfect matching in energy levels for this device configuration.

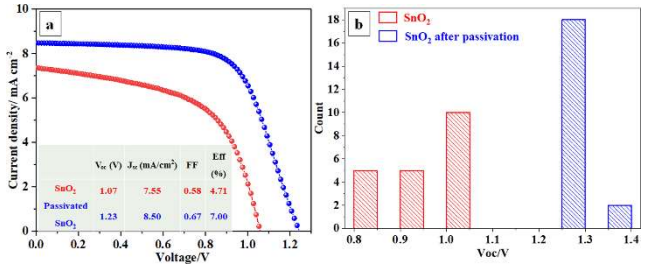

Fig. 4 (a) *J-V* curves of the champion PSCs based on bare or passivated SnO_2 ESL (inset table is the photovoltaic parameters); (b) V_{oc} distributions of two type PSCs (20 cells for each).

Fig. 4a displays the *J-V* curves of the champion $CsPbIBr_2$ PSCs with different ESLs and their corresponding photovoltaic parameters are shown as the inset in Fig. 4a. It is clear that the passivated SnO_2 based device is outperforming the bare SnO_2. The V_{oc}, short-circuit photocurrent (J_{sc}) and filling factor (FF) of the passivated SnO_2 based device are 1.23 V, 8.50 mA cm^{-2} and 0.67, respectively, resulting a high PCE of 7.00 %, with 0.16 V and 48.6% enhancement in V_{oc} and PCE when comparing with the bare SnO_2 based device (1.07 V and 4.73 %). All the measured J_{sc} in our experiments well matches the photocurrent density calculated from the incident photon-to-electron conversion efficiency (IPCE) spectra (Fig. S7). The higher J_{sc} might be partly attributed to the denser light absorber layer because of its stronger light absorption ability. While the bare SnO_2 based PSC has a little higher EQE values than those of the passivated one in the range of 300-400 nm, which could be attributed to the better transmittance property of the bare SnO_2 film in this range, as shown in the transmittance spectra of different SnO_2 films (Fig. S1). The stability output of the champion cells is measured in ambient air, in which the bias voltage is set at their respective maximum power points. As displayed in Fig. S8, the stabilized PCE of the passivated SnO_2 based device is estimated to be 6.45% after 130s continuous measurement, which is higher than that of the bare SnO_2 based device of 3.91%. At the same time, the passivated SnO_2 based device has a slight increase in PCE, while a slight decrease for the bare SnO_2 based device. This indicates the better output stability for the device with passivated SnO_2 as ESL. We summarized the performances of the $CsPbIBr_2$ based PSCs with carbon or Au electrode reported to date, as shown in Tab. S1. We found that the champion PCE (7.00 %) obtained for a passivated SnO_2 based solar cell in this work is comparable to those of the literature.

In order to verify the reproducibility of the high-performance passivated SnO_2 based PSCs, we fabricated 20 pieces of bare SnO_2 and passivated SnO_2 ESL-based solar cells, respectively, as listed in Tab. S2. We found that the PCEs of the most passivated SnO_2 based devices are in the range of 5.27 to 7.00 %, while all the bare SnO_2 based cells show PCEs lower than 4.71 %. Whilst, all the V_{oc} of the passivated SnO_2 based cells is above 1.20 V while the V_{oc} of the bare SnO_2 based devices distributed in the range from 0.85 to 1.07 V. The V_{oc} distributions of the PSCs on bare and passivated SnO_2 are shown in Fig. 4b. Thus our passivation method is highly reproducible in achieving high V_{oc}. More importantly, the highest V_{oc} of 1.31 V was achieved after SnO_2 surface passivation, which is higher than other reported $CsPbIBr_2$ PSCs (Tab. S1) and is one of the highest V_{oc} obtained for inorganic $CsPbX_3$ PSCs. Therefore, we can conclude that the passivation of SnO_2 ESL with the ultra-thin SnO_2 film is a promising approach to reduce E_{loss} for $CsPbIBr_2$ PSCs.

To completely understand the passivation effect of the SnO_2 film, various concentration of $SnCl_2$ solution were studied. It shows that too low concentration of $SnCl_2$ is ineffective in passivating the SnO_2 film as proven through its non-obvious enhancement in the performance (Fig. S9 and Tab. S3). In contract, a thicker SnO_2 passivation layer (high concentration) increases the series resistance of the device (Fig. S10). We also prepared a single SnO_2 layer on ITO using 0.1 M $SnCl_2$ precursor with the spin-coating speed of 2000 rpm. We found that its performance is compromised, as compared to the bare SnO_2 ESL based device (Fig. S9 and Tab. S3). Thus the reason for the reduced E_{loss} and enhanced performance of the passivated SnO_2 based solar cells lies in the interface modification, rather than the difference between the SnO_2 films prepared from SnO_2 colloid solution or $SnCl_2$ precursor.[8, 24, 25]

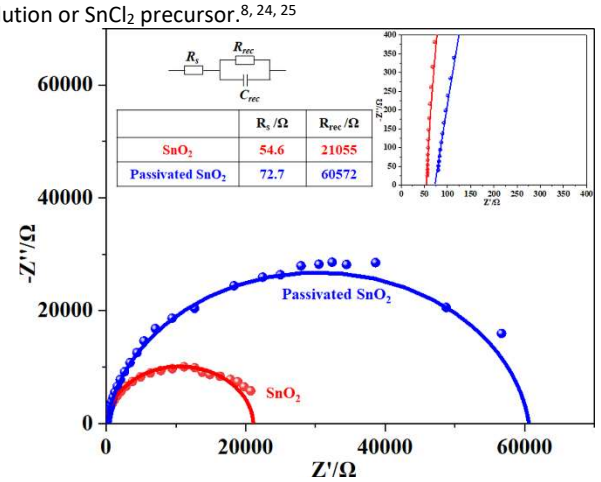

Fig. 5 Nyquist plots of PSCs based on bare or passivated SnO_2 in dark condition at a voltage of V_{oc}. Inset: the equivalent circuit, the enlarged high-frequency region, and table of simulated results.

The electrochemical impedance spectroscopy (EIS) measurements were carried out to investigate the interfacial charge transfer properties in the PSCs with SnO_2 ESL with or without passivation. The EIS were measured at an applied bias of V_{oc} in dark condition and the results are shown in Fig. 5. Generally, the high-frequency arc represents the transport process combining the transport resistance and the transport chemical capacitance, which are relating to the charge transporting from the cathode to the anode. While the arc at the low-frequency region represents the recombination resistance (R_{rec}) and the chemical capacitance (C_{rec}) at the interface of perovskite/SnO_2 and perovskite/carbon.[25, 26] It is clear that the device with passivated SnO_2 ESL shows larger R_{rec} (60572 Ω) than that of bare SnO_2 ESL based device (21055 Ω), which indicates that the recombination process in the former device is highly suppressed. Simultaneously, the former has a little larger series resistance (R_s) than that of the latter owing to its thicker SnO_2 film. We also measured the EIS of other devices with different ESLs, as shown in Fig. S10. We found that after passivation, the devices possess larger R_{rec} than that of the bare SnO_2 based device and the 0.1 M $SnCl_2$ passivation leads to highest R_{rec} (summarized in the table inset in Fig. S10), thus contributed for the best performance. While the device using SnO_2 ESL prepared by spin-coating 0.1 M $SnCl_2$ at 2000 rpm shows the smallest R_{rec}. In brief, this surface passivation decreases the recombination process at the interface between the perovskite and the ESL, which significantly improves the V_{oc} and PCE of the devices.

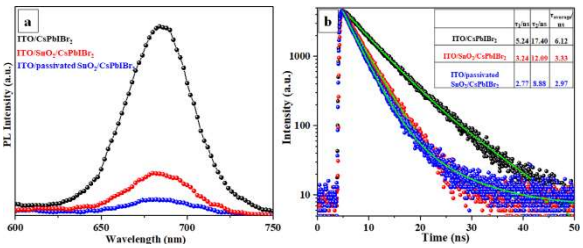

Fig. 6 (a) Steady-state photoluminescence (PL) spectra and (b) normalized transient PL decay profiles for $CsPbIBr_2$, bare SnO_2/$CsPbIBr_2$, and passivated SnO_2/$CsPbIBr_2$.

To better understand the effect of SnO_2 passivation on the electron extraction and transport mechanism, the steady-state PL and time-resolved PL (TRPL) measurements of the perovskite film on different substrates were conducted. Fig. 6a shows the PL spectra of ITO/$CsPbIBr_2$, ITO/SnO_2/$CsPbIBr_2$ and ITO/ passivated SnO_2/$CsPbIBr_2$ samples. The ITO/$CsPbIBr_2$ displays high PL intensity, which implies serious carrier recombination.[8] The ITO/ passivated SnO_2 /$CsPbIBr_2$ sample shows lower PL intensity than that of the ITO/SnO_2/$CsPbIBr_2$ sample, indicating stronger electron extraction ability from the perovskite film and lower recombination possibility.[27] Fig. 6b shows the TRPL spectra of the samples and the decay time is calculated via the exponential fits of the spectra. The parameters are listed in the table inserted in Fig. 6b. As shown in the table, when the $CsPbIBr_2$ is deposited on the bare ITO substrate, the PL decay times are 5.24 and 17.40 ns for τ_1 and τ_2, respectively. While the ITO/SnO_2/$CsPbIBr_2$ sample possesses the reduced PL decay time of 3.24 and 12.09 ns for τ_1 and τ_2, respectively. When the passivated SnO_2 ESL was used for the perovskite film deposition, both the τ_1 and τ_2 are further reduced to 2.77 and 8.88 ns, respectively. Moreover, the $CsPbIBr_2$ film on the passivated SnO_2 ESL has the smallest average decay time among the three samples. Thus the passivation of SnO_2 ESL can accelerate the electron injection rate from the perovskite film and suppress the charge recombination at the perovskite/ESL interface, resulting in higher V_{oc} and better performance.

Fig. S11 displays the hysteresis properties of both SnO_2 and passivated SnO_2 based $CsPbIBr_2$ PSCs. We found that both kinds of devices have severe hysteresis if compare with the organic-inorganic hybrid PSCs. The hysteresis index for the SnO_2 and passivated SnO_2 based device are 43% and 42.3%, respectively. Yibing Cheng and co-workers have explained this phenomenon by pointing out that there is iodide-rich phase segregation near the grain boundaries, forming clusters in $CsPbIBr_2$ film, which has a great influence on the ion migration.[17] Concentrated mobile ions generated by phase segregation pile up at the $CsPbIBr_2$/ESL interface, resulting in the formation of larger injection barriers and hampering electron extraction. This phenomenon exacerbates the hysteresis in $CsPbIBr_2$ PSCs. On the other hand, the relative small grains size with a large number of grain boundaries and compositional defects accompanying with one-step solution fabrication method might be other reasons for the severe hysteresis properties.[9, 28]

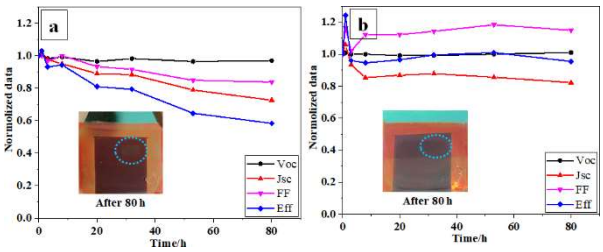

Fig. 7 Normalized photovoltaic parameters of the (a) bare and (b) passivated SnO_2 ESL based unencapsulated $CsPbIBr_2$ PSCs under continuously heating at 90 °C in air with the humility of 60-70%. Inset are the photographs of the two kinds of PSCs after heating for 80 hours.

It has been widely accepted that the degradation of perovskite occurs at the interface between the ESL and the perovskite materials.[29, 30] In order to investigate the effect of SnO_2 surface passivation on the device stability, we measured the thermal stability of the unencapsulated solar cells at 90 °C in the air with the relative humidity of 60-70 %. The time-dependent normalized V_{oc}, J_{sc}, FF, and PCE of the two type devices are shown in Fig. 7. It shows that the passivated SnO_2 based device has better durability than that of the bare SnO_2 based device. All the parameters of the two solar cells increase over the first one hour, which is recognized as interfacial ripening process with better charge transferability and improved crystallinity of the perovskite materials.[16, 31] During the subsequent tens of hours, the FF of the passivated SnO_2 based device kept at a higher level than the initial value, while the J_{sc} decreases obviously relative to the initial value. After 80 hours, the passivated device could still maintain 95.5% of its initial performance, which is much higher than that of the bare SnO_2 based device (58.3%). Moreover, we found that after long hours of light exposure, the appearance of the active area of the bare SnO_2 changes when viewing from the back side, as shown in Fig. 7a (inset), while this phenomenon was not observable for the passivated SnO_2 based device. Thus there should be some undesired photochemical reactions at the bare SnO_2/perovskite interface, such as the light and interface defects-induced halide migration in the $CsPbIBr_2$ film, that impede the high performance.[32, 33] Hence the SnO_2 surface modification can help to avoid the photochemical reactions and improve the thermal stability of inorganic PSCs.

Moreover, we studied the room-temperature phase stability of the $CsPbIBr_2$ perovskite materials. The measurements were carried out at 25 °C in the air at a relative humidity of 65 %. The results of the $CsPbIBr_2$ deposited on passivated SnO_2 film are shown in Fig. S12. It shows that $CsPbIBr_2$ is very unstable where the film changed from red to transparent quickly within 80 min. From the time-dependent XRD patterns of the sample, we observed that the phase changes from the photo-active α phase to non-photoactive δ phase after 80 min.[10] There is no obvious difference in phase stability for the perovskite film deposited on SnO_2 ESL with or without passivation at room temperature because the phase transition is mainly caused by water. While after the re-heating process in air, the transparent film re-transformed to red color film, meaning reversible phase transition property, which is in accordance with Peidong Yang's research.[34] Therefore, the room-temperature phase stability of $CsPbX_3$ perovskite materials, especially for the halide-rich phases, is one of the most important aspects that require prompt addresses.

Conclusions

In conclusion, our work has demonstrated an efficient interface engineering method of SnO_2 ESL passivation, which aims to reduce the energy loss of the all-inorganic Cs-based PSCs. We found that the passivation of SnO_2 not merely effectively decreases the recombination process at the interface between the $CsPbIBr_2$ perovskite and the SnO_2, but also accelerates the electron extraction efficiency from the perovskite film. After passivation, the efficiency was dramatically enhanced and a high V_{oc} of 1.31 V was achieved. The thermal stability of the passivated SnO_2 based devices highly outperformed the bare SnO_2 based solar cells. This work has proven that energy loss occurred in all-inorganic PSCs can be overcome through the interface engineering. We believe that this method is highly applicable to other PSCs for decreasing the E_{loss}.

Conflicts of interest

There are no conflicts to declare.

Acknowledgments

This work was supported by the Grant-in-Aid for Scientific Research (KAKENHI) program, Japan (C, Grant Number 15K05597) and Takahashi Industrial and Economic Research Foundation (Takahashi Grant Number 06-003-154). The authors would like to thank the Research Centre for Solar Light Energy Conversion, Kyushu Institute of Technology for their support.

References

1. A. Kojima, K. Teshima, Y. Shirai and T. Miyasaka, *J. Am. Chem. Soc.*, 2009, **131**, 6050.
2. https://www.nrel.gov/pv/assets/pdfs/pv-efficiencies-07-17-2018.pdf.
3. M. L. Petrus, J. Schlipf, C. Li, T. P. Gujar, N. Giesbrecht, P. Müller‐Buschbaum, M. Thelakkat, T. Bein, S. Hüttner and P. Docampo, *Adv. Energy Mater.*, 2018, **8**, 1703396.
4. Q. Jiang, Z. Chu, P. Wang, X. Yang, H. Liu, Y. Wang, Z. Yin, J. Wu, X. Zhang and J. You, *Adv. Mater.*, 2017, **29**, 1703852.
5. N. J. Jeon, H. Na, E. H. Jung, T.-Y. Yang, Y. G. Lee, G. Kim, H.-W. Shin, S. I. Seok, J. Lee and J. Seo, *Nat. Energy*, 2018, **3**, 682.
6. N.-K. Kim, Y. H. Min, S. Noh, E. Cho, G. Jeong, M. Joo, S.-W. Ahn, J. S. Lee, S. Kim and K. Ihm, *Sci. Rep.*, 2017, **7**, 4645.
7. G. Zhou, J. Wu, Y. Zhao, Y. Li, J. Shi, Y. Li, H. Wu, D. Li, Y. Luo and Q. Meng, *ACS Appl. Mater. Inter.*, 2018, **10**, 9503.
8. L. Yan, Q. Xue, M. Liu, Z. Zhu, J. Tian, Z. Li, Z. Chen, Z. Chen, H. Yan and H. L. Yip, *Adv. Mater.*, 2018, **30**, 1802509.
9. W. Zhu, Q. Zhang, D. Chen, Z. Zhang, Z. Lin, J. Chang, J. Zhang, C. Zhang and Y. Hao, *Adv. Energy Mater.*, 2018, 1802080.
10. P. Wang, X. Zhang, Y. Zhou, Q. Jiang, Q. Ye, Z. Chu, X. Li, X. Yang, Z. Yin and J. You, *Nat. Commun.*, 2018, **9**, 2225.
11. H. Bian, D. Bai, Z. Jin, K. Wang, L. Liang, H. Wang, J. Zhang, Q. Wang and S. F. Liu, *Joule*, 2018, **2**, 1500.
12. J. Duan, Y. Zhao, B. He and Q. Tang, *Small*, 2018, **14**, 1704443.
13. Y. Wang, T. Zhang, M. Kan and Y. Zhao, *J. Am. Chem. Soc.*, 2018, **140**, 12345.
14. G. E. Eperon, G. M. Paterno, R. J. Sutton, A. Zampetti, A. A. Haghighirad, F. Cacialli and H. J. Snaith, *J. Mater. Chem. A*, 2015, **3**, 19688.
15. J. Liang, Z. Liu, L. Qiu, Z. Hawash, L. Meng, Z. Wu, Y. Jiang, L. K. Ono and Y. Qi, *Adv. Energy Mater.*, 2018, 1800504.
16. J. Liang, P. Zhao, C. Wang, Y. Wang, Y. Hu, G. Zhu, L. Ma, J. Liu and Z. Jin, *J. Am. Chem. Soc.*, 2017, **139**, 14009.
17. W. Li, M. U. Rothmann, A. Liu, Z. Wang, Y. Zhang, A. R. Pascoe, J. Lu, L. Jiang, Y. Chen and F. Huang, *Adv. Energy Mater.*, 2017, **7**, 1700946.
18. N. Li, Z. Zhu, J. Li, A. K. Y. Jen and L. Wang, *Adv. Energy Mater.*, 2018, 1800525.
19. G. Yang, H. Lei, H. Tao, X. Zheng, J. Ma, Q. Liu, W. Ke, Z. Chen, L. Xiong and P. Qin, *Small*, 2017, **13**, 1601769.
20. C. Liu, W. Li, J. Chen, J. Fan, Y. Mai and R. E. Schropp, *Nano Energy*, 2017, **41**, 75.
21. Q. Ma, S. Huang, X. Wen, M. A. Green and A. W. Ho‐Baillie, *Adv. Energy Mater.*, 2016, **6**, 1502202.
22. R. J. Sutton, G. E. Eperon, L. Miranda, E. S. Parrott, B. A. Kamino, J. B. Patel, M. T. Hörantner, M. B. Johnston, A. A. Haghighirad and D. T. Moore, *Adv. Energy Mater.*, 2016, **6**, 1502458.
23. X. Ren, D. Yang, Z. Yang, J. Feng, X. Zhu, J. Niu, Y. Liu, W. Zhao and S. F. Liu, *ACS Appl. Mater. Inter.*, 2017, **9**, 2421.
24. J. Song, E. Zheng, X.-F. Wang, W. Tian and T. Miyasaka, *Sol. Energy Mater. Sol. Cells*, 2016, **144**, 623.
25. J. Ma, G. Yang, M. Qin, X. Zheng, H. Lei, C. Chen, Z. Chen, Y. Guo, H. Han and X. Zhao, *Adv. Sci.*, 2017, **4**, 1700031.
26. Y. Hou, X. Chen, S. Yang, C. Li, H. Zhao and H. G. Yang, *Adv. Funct. Mater.*, 2017, **27**, 1700878.
27. T. C. Sum and N. Mathews, *Energy Environ. Sci.*, 2014, **7**, 2518.
28. J. Huang, Y. Yuan, Y. Shao and Y. Yan, *Nat. Rev. Mater.*, 2017, **2**, 17042.
29. K. K. Wong, A. Fakharuddin, P. Ehrenreich, T. Deckert, M. Abdi-Jalebi, R. H. Friend and L. Schmidt-Mende, *J. Phys. Chem. C*, 2018, **122**, 10691.
30. S. Ito, S. Tanaka, K. Manabe and H. Nishino, *J. Phys. Chem. C*, 2014, **118**, 16995.
31. Q. Dong, M. Wang, Q. Zhang, F. Chen, S. Zhang, J. Bian, T. Ma, L. Wang and Y. Shi, *Nano energy*, 2017, **38**, 358.
32. S. Draguta, O. Sharia, S. J. Yoon, M. C. Brennan, Y. V. Morozov, J. M. Manser, P. V. Kamat, W. F. Schneider and M. Kuno, *Nat. Commun.*, 2017, **8**, 200.
33. W. Zhang, V. M. Burlakov, D. J. Graham, T. Leijtens, A. Osherov, V. Bulović, H. J. Snaith, D. S. Ginger and S. D. Stranks, *Nat. Commun.*, 2016, **7**, 11683.
34. J. Lin, M. Lai, L. Dou, C. S. Kley, H. Chen, F. Peng, J. Sun, D. Lu, S. A. Hawks and C. Xie, *Nat. Mater.*, 2018, **17**, 261.